RHex - A Simple and Highly Mobile Hexapod Robot

Uluç Saranli*, Martin Buehler† and Daniel E. Koditschek*

*Department of Electrical Engineering and Computer Science
The University of Michigan, Ann Arbor, MI 48109-2110, USA
†Center for Intelligent Machines
McGill University, Montreal, QC H3A 2A7, Canada

Abstract

In this paper, we describe the design and control of RHex, a power autonomous, untethered, compliant-legged hexapod robot. RHex has only six actuators — one motor located at each hip — achieving mechanical simplicity that promotes reliable and robust operation in real-world tasks. Empirically stable and highly maneuverable locomotion arises from a very simple clock-driven, open-loop tripod gait. The legs rotate full circle, thereby preventing the common problem of toe stubbing in the protraction (swing) phase. An extensive suite of experimental results documents the robot's significant "intrinsic mobility" — the traversal of rugged, broken and obstacle ridden ground without any terrain sensing or actively controlled adaptation. RHex achieves fast and robust forward locomotion traveling at speeds up to one body length per second and traversing height variations well exceeding its body clearance.

I. Introduction

Fig. 1. *The RHex experimental platform (ai.eecs.umich.edu/RHex).*

In this paper we report on a power autonomous legged vehicle, RHex, Figure 1, that easily traverses terrain approaching the complexity and diversity of the natural landscape. Table I subtantiates in part our belief that this machine breaks the speed record to date for power autonomous legged robot locomotion over uneven terrain by a considerable margin[1]. RHex travels at speeds approaching one body length per second over height variations exceeding its body clearance (see Extensions 1 and 2). Moreover, RHex does not make unrealistically high demands of its limited energy supply (two 12V sealed lead-acid batteries in series, rated at 2.2Ah): at the time of this writing (Spring 2000), RHex achieves sustained locomotion at maximum speed under power autonomous operation for more than fifteen minutes.

TABLE I
Summary of Published Performance Reports: Hexapedal Robot

Name	L(m)[b]	M(kg)[b]	V(m/s)[b]	V/L
CW Robot II [11]	0.5	1	0.083	0.16
Dante II [5]	3	770	0.017	0.006
Atilla[a] [4]	0.36	2.5	0.03	0.083
Genghis[a] [3]	0.39	1.8	0.038	0.097
ASV[a] [29]	5	3200	1.1	0.22
Boadicea [6]	0.5	4.9	0.11	0.22
Sprawlita [12]	0.17	0.27	0.42	2.5
RHex[a]	0.53	7	0.55	1.04

[a] Power autonomous
[b] L: Body length, M: Robot mass, V: maximum speed

The robot's design consists of a rigid body with six compliant legs, each possessing only one independently actuated revolute degree of freedom. The attachment points of the legs as well as the joint orientations are all fixed relative to the body. The use of spoked wheels (or even highly treaded wheels) is of course an old idea. Compa-

This work is supported in part by DARPA/ONR Grant N00014-98-1-0747

[1] Unfortunately, there is not enough performance detail documented in the published robotics literature to unconditionally establish this claim. To the best of our knowledge, the very few robots that have been demonstrated to negotiate uneven terrain at all, travel at speeds far less than those we report here.

rable morphologies such as rimless wheels [13] or single spoked wheels [22] have been previously proposed for mobile platforms. Some compliant legged designs have been proposed for toys [20], and some rigid rimless wheeled designs have actually been commercialized by the toy industry [26]. However, the major difference between a single leg and a wheel with more than two spokes arises from the far greater range of control over the ground reaction forces (GRF) that the former affords relative to the latter. Wheels afford control primarily over the horizontal component of the GRF (assuming flat ground) through friction, incurring an essentially uncontrolled concomittant vertical component. In contrast, a leg, by admitting selection over the angle of contact, yields a GRF whose direction as well as magnitude may be substantially controlled. As soon as multiple spokes are added, the inter-spoke angle restricts the range of contact angles, thereby diminishing control affordance. Our design preserves the possiblity of achieving full GRF range while adding the virtues of tuned compliance, heretofore associated only with wheels.

Fig. 2. *Comparative views of locomotion in the rough: the cockroach* Blaberus discoidalis *(top photo, courtesy of R. J. Full [14]) runs at 3.7 body lengths (∼24 cm) per second [15], whereas RHex (bottom photo) presently runs at only one body length (∼50 cm) per second over comparably scaled broken terrain (see Extensions 3 and 4).*

The closest extant robots, one significant source of inspiration for the RHex design, are the second author's Scout class quadrupeds (www.cim.mcgill.ca/˜arlweb) [9, 10, 28] that also feature compliant legs, and reduce mechanical complexity by the restriction of one actuator per leg[2]. The central difference with respect to this design is the possibility of recirculating — i.e., treating the singly actuated leg as a single spoked "rimless wheel". A second key design influence whose careful consideration exceeds the scope of this paper arises from biomechanics. R.J. Full's video of a Blaberus cockroach racing seemingly effortlessly over the rough surface illustrated in Figure 2, was shown at an interdisciplinary meeting [27] motivating and initiating the development of RHex. The present design may be seen as instantiating the notion of a "preflex" [8] — implemented here in the clock driven mechanically self stabilizing compliant sprawled posture mechanics that Full proposed[3] [15]. The notion of a "clock driven" mechanism arises in our choice of an controller to derive appropriate advantage of RHex's mechanical design. At the time of this writing, RHex operates by tracking (via local PD contol) at each hip joint a copy of the reference trajectory depicted in Figure 4 that enforces an alternating tripod gait in an otherwise open loop manner. The two tripods are driven in relative antiphase. The three legs of a tripod are driven simultaneously through a slow "retraction" phase, putatively corresponding to ground contact, followed by a fast "protraction" phase designed to recirculate the legs away from the the ground around the axle just in time to reach the next "retraction" phase, putatively as the opposing tripod begins its "protraction" by rotating away from ground contact. No design we are aware of has heretofore incorporated this combination of controller simplicity, leg compliance, limited actuation and overall morphology, and no previously implemented legged vehicle has achieved the performance we now report.

Table I (modeled on, but extended from [6]) summarizes performance data for previous hexapedal vehicles respecting which we are aware of documented performance, with citations to refereed publications. It would be of considerable interest to compare across a broader range of machines. Unfortunately, it is not straightforward to normalize against morphology. For example, "body lengths per second" is clearly not an appropriately normalized measure of bipedal speed. We look forward to the eventual adoption of appropriately general performance metrics for legged locomotion within the robotics research community. For the present, it seems most useful to compare the design of RHex with some of its more closely related forebears.

One of the better documented, faster, power autonomous hexapods, the OSU adaptive suspension vehicle (ASV) was designed to operate in the statically stable regime. The deleterious consequences of design complexity have been observed in Dante II [5], a tethered hexapod whose exposure to severe environmental conditions have apparently been the most extreme of any robot yet documented in the

[2]Scout II travels at just under two bodylengths per second, but traverses only level ground.

[3]See [2] for a technical discussion of some aspects relating the bioinspiration behind this design to its performance.

archival literature. On a smaller scale, there have been many platforms inspired by insect locomotion [3, 4, 6], all designed for statically stable gaits. Their speeds were thus limited even though their design afforded greater kinematic freedom over limb motions. A notable exception in the smaller scale is Sprawlita [12], a tethered hexapod which can achieve a very impressive 2.5 body lengths per second locomotion speed as a result of its careful (compliant leg) design, and construction (offboard pneumatic actuation and small size).

For most of these machines, rough terrain performance and obstacle crossing capabilities are not carefully documented in the literature. There are only a few examples where such capabilities are reported in detail [5, 29], but even these are not suitable for assessing relative performance due to differences in scale and the lack of a consistent set of experiments and measures. Without more or less uniform standards of reporting, it becomes very difficult to test the claim that the relative speed (we use body lengths per second), relative endurance (we use specific resistance but also provide actual run-time data as well), relative mobility (we provide a metric characterization of the various terrain features) of one design is superior to another. Thus, beyond the specifics of design and performance, we believe that the paper makes a distinct contribution to the robotics literature by establishing new standards of rigor in empirical performance reporting for legged vehicles.

In summary, we believe this new design opens up a large range of new possibilities for control of locomotion, while still meeting the constraints imposed by contemporary actuation and energy storage technology on engineering autonomous robotic platforms. At the present time, we are unable to provide a mathematically informed analysis of how and why RHex performs over the range of reported behaviors. Instead, in this first archival paper, we present careful empirical documentation of a narrow but very useful behavioral suite — a base range of locomotion capabilities at relatively high speeds over relatively challenging terrain — and observe that no other power autonomous legged design has ever before been demonstrated to exhibit a comparable breadth of mobility behaviors.

II. Design and Modeling

A. Design Concept and Morphology

In all robotics applications, mechanical complexity is one of the major sources of failure and considerably increases the cost. Our design emphasizes mechanical simplicity and thereby promotes robustness. Autonomy, a critical component of our aspiration toward real-world tasks in unstructured environments outside the laboratory, imposes very strict design constraints on the hardware and software components. It is often impossible to achieve with simple modifications to a system otherwise designed for non-autonomous operation. These constraints also justify our preference for overall simplicity — in particular towards minimizing the amount of actuation and limited reliance on sensing.

Our design, depicted in Figure 3, consists of a rigid body with six compliant legs, each possessing only one independently actuated revolute degree of freedom. The attachment points of the legs as well as the joint orientations are all fixed relative to the body.

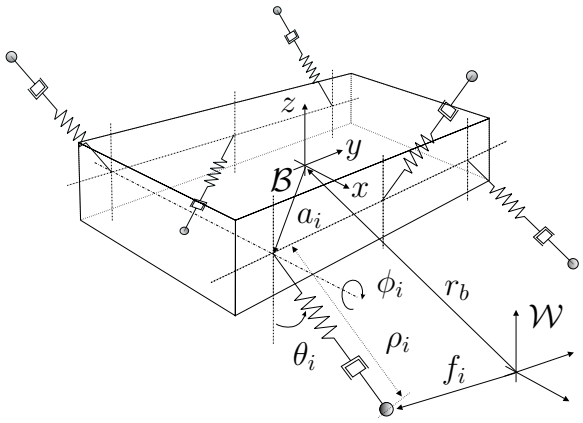

Fig. 3. *The compliant hexapod design.*

This configuration admits an alternating tripod gait for forward and backward locomotion, and possibly other more elaborate behaviors such as leaping, stair climbing etc. Moreover, the symmetry of this idealized model allows identical upside-down operation and imposes no restrictions on forward directionality. We explore some of this behavioral repertoire both in simulation and experimentally in Section IV and Section V, respectively.

B. The Compliant Hexapod Model

In this section, we present a dynamical model of the morphology described in the previous section. Prior to the construction of the experimental prototype, this model enabled us to assess the viability of the design through simulation studies. Augmented with the actuator model of Section IV-A, it proved to be an invaluable tool in the design process.

Two reference frames, $\mathcal{B}$ and $\mathcal{W}$ are defined in Figure 3, the former attached to the hexapod body and the latter an inertial frame where the dynamics are formulated. In $\mathcal{B}$, we define the $+y$ direction to be *forward* and the $+x$ direction to be the the *right side* of the robot. The position and orientation of the rigid body are described by $\mathbf{r_b} \in R^3$ and $\mathbf{R_b} \in SO(3)$, respectively, expressed in $\mathcal{W}$. Table II details the notation used throughout the paper.

Each leg is assumed to be massless and has three degrees of freedom. The leg state is described in spherical coordinates $[\theta_i, \phi_i, \rho_i]^T$ whose origin is at $\mathbf{a_i}$ in the body frame[4].

[4]Note that $(\mathbf{r_b}, \mathbf{R_b})$, $\mathbf{v_i}$ and $\mathbf{f_i}$ are related through the coordinate transformation $-\mathbf{R_b}(\mathbf{a_i} + \overline{\mathbf{v}}_\mathbf{i}) = \mathbf{f_i} + \mathbf{r_b}$

TABLE II
NOTATION

States	
$\mathbf{r_b}$, $\mathbf{R_b}$	body position and orientation
α	body yaw angle
Leg states and parameters	
$\mathbf{a_i}$	leg attachment point in $\mathcal{B}$
$\mathbf{f_i}$	toe position in $\mathcal{W}$
$\mathbf{v_i}$	$:= [\theta_i, \phi_i, \rho_i]^T$ leg state in spherical coordinates
$\overline{\mathbf{v}}_\mathbf{i}$	$:= [v_{x_i}, v_{y_i}, v_{z_i}]^T$ leg state in cartesian coordinates
leg_i	stance flag for leg i
Forces and Torques	
F_{r_i}	radial leg spring force
τ_{θ_i}	bend torque in θ_i direction
τ_{ϕ_i}	hip torque in ϕ_i direction
Controller Parameters	
t_c	period of rotation for a single leg
t_s	duration of slow leg swing
ϕ_s	leg sweep angle for slow leg swing
ϕ_o	leg angle offset
$\mathbf{u}$	$:= [t_c, t_s, \phi_s, \phi_o]$ control vector
$\Delta\phi_o$	differential change in ϕ_o for turning
Δt_s	differential change in t_s for turning.

B.1 Equations of Motion

Our formulation of the equations of motion for the hexapod model is based on individually incorporating the ground reaction forces at each leg. To this end, it will suffice to analyze a generic leg parametrized by its attachment and touchdown points, $\mathbf{a_i}$ and $\mathbf{f_i}$, respectively. As a consequence of the assumption that the leg is massless, the rigid body experiences the ground reaction force on the leg, resulting in effective force and torque vectors acting on the center of mass. For each leg $i = 1, ..., 6$, following projections on $\mathcal{B}$, we have,

$$\mathbf{F_i} = \begin{bmatrix} -\cos\theta_i \sin\phi_i & \sin\theta_i \sin\phi_i & -\cos\phi_i \\ \sin\theta_i & \cos\theta_i & 0 \\ \cos\theta_i \cos\phi_i & -\sin\theta_i \cos\phi_i & -\sin\phi_i \end{bmatrix} \cdot \begin{bmatrix} F_{r_i} \\ \tau_{\theta_i}/\rho_i \\ \tau_{\phi_i}/(\rho_i \cos\theta_i) \end{bmatrix}$$

$$\tau_\mathbf{i} = (\overline{\mathbf{v}}_\mathbf{i} + \mathbf{a_i}) \times \mathbf{F_i}$$

which are the force and torque contributions of a single leg to the overall system dynamics, respectively. The cumulative effect of all the legs on the body is simply the sum of the individual contributions from the legs in contact with the ground, together with the gravitational force.

$$\mathbf{F_T} = \begin{bmatrix} 0 & 0 & -mg \end{bmatrix}^T + \mathbf{R_b} \sum_{i=1}^{6} leg_i \mathbf{F_i} \quad (1)$$

$$\tau_\mathbf{T} = \mathbf{R_b} \sum_{i=1}^{6} leg_i \tau_\mathbf{i} \quad (2)$$

(3)

The contact states of the legs are indicated by leg_i. In consequence, the dynamics of the hexapod are governed by the standard rigid body dynamics under external torque and force inputs [18]. Note also that, the discrete transitions in the contact states of the legs result in a hybrid dynamical system, whose behavior can be substantially different than that of its continuous constituents alone.

III. Control Strategy

The present prototype robot has no external sensors by which its body state may be estimated. Thus, in our simulations and experiments, we have used joint space closed loop ("proprioceptive") but task space open loop control strategies. The algorithms that we describe in this section are tailored to demonstrate the intrinsic reliability of the compliant hexapod morphology and emphasize its ability to operate without a sensor-rich environment. Specifically, we present a four-parameter family of controllers, that yields translation and turning of the hexapod on flat terrain, without explicit enforcement of quasi-static stability. In Section V-C, we demonstrate the capabilities of this family of controllers on our experimental platform, over a wide range of terrain conditions, from flat terrain to a rough, broken surface.

All controllers generate periodic desired trajectories for each hip joint, which are then enforced by six local PD controllers (one for each individual hip actuator). In this respect, the present controller family represents one near-extreme along the spectrum of possible control strategies, ranging from purely feedforward (i.e., taking no notice of body state), to purely feedback (i.e., producing torque solely in reaction to leg and rigid body state). It seems likely that neither one of these extremes is best and a combination should be adopted. The simulations and experiments presented in this paper attempt to characterize the properties associated with the sensorless feedforward extreme, which, when RHex has been endowed with sensors, we hope to complement with feedback to explore the aforementioned range.

An alternating tripod pattern governs both the translation and turning controllers, whereby the legs forming the left and right tripods are synchronized with each other and are 180^o out of phase with the opposite tripod, as shown in Figure 4.

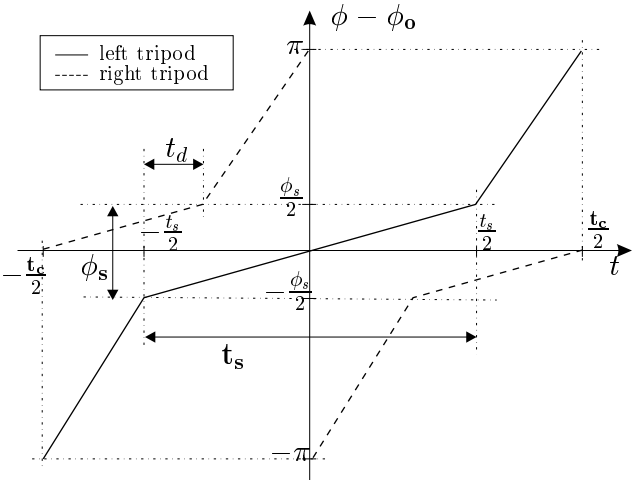

Fig. 4. *The motion profiles for left and right tripods.*

A. The Forward Alternating Tripod Gait

The open loop controller's target trajectories for each tripod are periodic functions of time, parametrized by four variables: t_c, t_s, ϕ_s and ϕ_o. In a single cycle, both tripods go through slow and fast swing phases, covering ϕ_s and $2\pi - \phi_s$ of the complete rotation, respectively. The period of both profiles is t_c. In conjunction with t_s, it determines the duty factor of each tripod, with respect to the duration of their slow and fast phases. The time of "double support" t_d (where all six legs are in their slow phases, but possibly not all of them touching the ground) is hence determined by the duty factors of both tripods. Finally, the ϕ_o parameter offsets the motion profile with respect to the vertical (see Figure 4). Note that both profiles are illustrated to be monotonically increasing in time; but they can be negated to obtain backward locomotion.

Control of locomotion is achieved by modifying these parameters for a particular desired behavior during locomotion. In Section IV, our simulation studies reveal correlations of these parameters with certain behavioral attributes.

B. Turning

We have developed two different controllers for two qualitatively different turning modes: turning in place and turning during translation. These controllers are inspired by differential turning in wheeled and tracked vehicles, where opposite perturbations to contralateral actuators result in a net rotation of the body on the plane. Analytical understanding of this behavior in the context of our design awaits careful mathematical treatment of RHex's dynamics as well as accurate models of ground contact.

The controller for turning in place employs the same leg profiles as for forward locomotion except that contralateral sets of legs rotate in opposite directions. This results in the hexapod turning in place in the direction determined by the rotational polarity of the left and right sets of legs. Note that the tripods are still synchronized internally, maintaining three supporting legs on the ground. Similar to the control of the forward locomotion speed, the rate of turning depends on the choice of the particular motion parameters, mainly t_c and ϕ_s.

In contrast, we achieve turning during forward locomotion by introducing differential perturbations to the forward running controller parameters for contralateral legs. In this scheme, t_c is still constrained to be identical for all legs, which admits differentials in the remaining profile parameters, ϕ_o and t_s, while ϕ_s remains unchanged. Two new gain parameters, Δt_s and $\Delta\phi_o$ are introduced. Turning right (towards $+x$ in the coordinate system of Figure 3, defining $+y$ as forward) is achieved by using $\mathbf{u}_l = [t_c, t_s + \Delta t_s, \phi_s, \phi_o + \Delta\phi_o]$ and $\mathbf{u}_r = [t_c, t_s - \Delta t_s, \phi_s, \phi_o - \Delta\phi_o]$ for the legs on the left and right sides, respectively.

IV. Simulation Studies

Our simulation studies in this section use the dynamical model described in Section II-B, together with an actuator model to demonstrate the feasibility of basic locomotion behaviors of our design under practical actuation limitations. The presented results provide a proof of concept for the design, justifying the building of our prototype and the extensive experiments of later sections. In order to limit the scope of the paper to an appropriate length, however, we have excluded impact of these models and the resulting simulation tools in refining the kinematic and dynamical parameters of our experimental prototype.

A. Actuator Model

The model of Section II-B does not impose any constraints on the choice of the hip torques τ_{ϕ_i}. In practice, however, torque limitations are one of the major challenges in the design of autonomous legged vehicles, even for statically stable modes of operation. In order to capture this aspect of our design space in the subsequent simulation studies, we incorporate a simple model of the hip actuation.

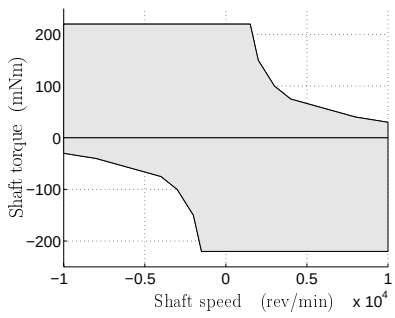

Fig. 5. *Torque characteristics for the Maxon RE118751 20W DC motor, reproduced from the manufacturer's datasheet. The shaded band illustrates the range of torque deliverable by the motor.*

Figure 5 portrays the experimentally measured torque-speed characteristics for the DC motors used in our experimental platform. The shaded band captures the range of torque deliverable by the motor at any particular speed[5]. Our simulations incorporate this model by saturating hip torque command outputs of the local PD controllers as a function of the leg angular velocity.

B. Simulation Environment

All the simulation results of the next section are produced by *SimSect*, a simulation environment that we have created primarily for the study of the compliant hexapod platform [31]. SimSect can efficiently and accurately deal with the hybrid nature of the model resulting from discrete ground contact model, preserving the relatively simple dynamics of the continuous model.

The hexapod simulation with *SimSect* uses the same dimensions and body mass as our experimental platform (see Section V). However, some of the dynamical parameters used in the simulations, including the leg spring and damping constants, and the ground friction coefficient are not experimentally verified and are likely to be different from their actual values. Nevertheless, the relatively accurate match between the simulations and the experimental platform regarding their morphology and mass parameters still admit qualitative comparisons of behavior.

C. Simulation Results

In this section, we verify in simulation that the controllers of Section III are able to produce fast autonomous forward locomotion of the hexapod platform.

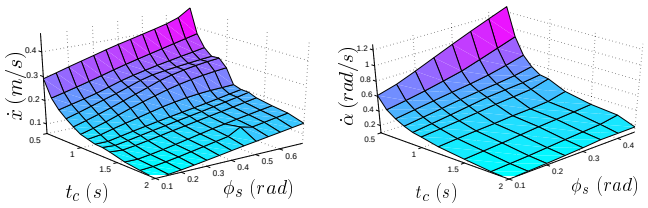

(a) (b)

Fig. 6. *(a) Average forward velocity $\dot{y}$ as a function of t_c and ϕ_s over 5s of operation, during which the robot always settled down to an approximately periodic trajectory. Remaining controller parameters are chosen as $t_s = t_c/2$, $\phi_o = 0$. (b) Average in-place turning yaw rate $\dot{\alpha}$ as a function of t_c and ϕ_s over 5s of operation.*

Figure 6 shows the the forward velocity (a) and the turning yaw rate (b) as functions of controller parameters t_c and ϕ_s. Although the remaining parameters t_s and ϕ_o have considerable effect on both the body oscillations during locomotion as well as the forward velocity, through manual tuning, we identified certain values for them to yield good performance in most cases. As a consequence, throughout these simulations, ϕ_o is kept constant and t_s is chosen to be half the stance time. Nevertheless, it is clear that proper tuning of all four controller parameters is necessary to achieve the smoothest and fastest locomotion performance. The effects of a hand tuned, intuitively "best" choice for a given t_c and ϕ_s is demonstrated in Figure 7 and the associated Extension 5, a typical forward translation with an average velocity of $0.55m/s$.

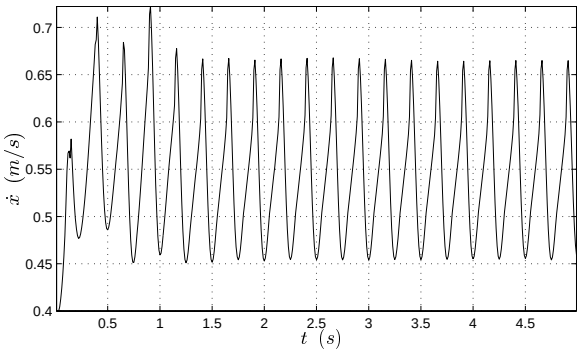

Fig. 7. *Forward body velocity for a simulation run with $t_c = 0.5s$, $\phi_s = 0.7rad$, $t_s = 0.3s$ and $\phi_o = 0.03rad$.*

These results suggest the opportunities for considerably improved performance resulting from the introduction of feedback to regulate the forward locomotion and turning yaw rate of the compliant hexapod platform. We sketch our approach to these future opportunities in the conclusion.

V. Experimental Platform

A. Hardware Description

We have built an experimental platform (Figure 1) as an instantiation of the design concepts of Section II-A. RHex is an autonomous hexapod robot with compliant legs, very close to the model described in Section II-B. All the computational and motor control hardware is on board, together with two Panasonic 12V 2.2Ah sealed lead-acid batteries for power autonomous operation. A PC104 stack with a 100 MHz Intel 486 microprocessor, together with several I/O boards performs all the necessary computation and implements the controllers of Section III. A remote control unit provides the user input for giving higher level commands such as the forward speed, and turning direction, presently via a joystick.

Each leg is directly actuated by a Maxon RE118751 20W brushed DC motor combined with a Maxon 114473 two-stage 33:1 planetary gear [24], delivering an intermittent stall torque of 6 Nm. The motor angle, and thus the leg angles, are controlled via 1 kHz software PD control loops. The control software also features several safety measures, including fault detection for the encoders, estimation of the

[5]Note that the we have conservatively approximated the DC motor characteristics by assuming constant maximum torque for second and fourth quadrants.

rotor temperatures to avoid motor damage, and a watchdog timer which disables the motors and resets the computer in case of software failures.

The main body measures 53x20x15 cm, and roughly matches the symmetries of the ideal model, except for the slightly lower center of mass and the larger length of the bottom side. The legs are made from 1 cm diameter Delrin rods and are "C" shaped to increase compliance in the radial direction and permit easy clamping to the gear shaft (see Extension 6). The leg length is 17.5 cm, measured as the vertical distance from ground to the gear shaft when standing up. We experimentally measured their compliance to be approximately 4500 N/m in their expected operating region. The encoder/motor/gear stacks protrude from the main body and the maximum widths of the front and back legs amount to 39.4 cm, measured at half the leg length. To provide clearance for the rotating front and back legs, the motors for the middle legs are further offset and result in a maximum width of 52 cm. The total mass of the robot is 7 kg with each leg contributing only approximately 10 g.

B. Visual Measurement Apparatus

Absent any inertial sensing on RHex, we devised a simple visual tracking system to record the robot's position and orientation in the sagittal (obstacle crossing experiments) and the horizontal (turning and rough surface experiment) planes. Four Light Emitting Diodes (LEDs) were attached to the robot's body and a set of stationary calibration LEDs were placed close to the extremes of the camera's field of view. The experiments were then conducted in complete darkness, which provided for very high contrast recordings of the LED markers. Thanks to this greatly simplified visual data, standard computer vision algorithms were then employed to extract the planar robot position and orientation up to a 1% accuracy in the average velocity computations.

C. Experimental Results

In the sequel, we will document the robot's speed over various terrains, its maneuverability, obstacle crossing capability, and payload. Furthermore, energy efficiency and runtime are critical performance criteria for any untethered robot. Thus the energetic performance of the robot is carefully documented, but it must be noted that at the time of this writing, no efforts have been made to optimize it. All experiments — except the random obstacles experiment, Figure 12, Section B-D — were run untethered and we document the average power consumption, based on recordings of the battery voltage and current.

To measure energy efficiency we use the "Specific Resistance" [17], $\varepsilon = P/(mgv)$, based on the robot's weight, mg, and its average power consumption, P, at a particular speed, v. Specific resistance was originally used to compare the energy efficiency of animals of vastly different sizes, where the average power measured the rate of metabolic energy expenditure, based on oxygen consumption. The same measure has been used to compare the energy efficiency of a range of different robots [1, 19, 21, 35]. Unfortunately, attention to energy efficiency and its reporting is fairly rare in robotics, and not consistent. For example, the power, if documented at all, is given as the mechanical power delivered by the actuators, the peak mechanical power of the main power source, or the total electrical power consumption. Therefore, quantitative energetic comparisons of past robots are not always precise. For electrically actuated mobile robots like RHex it makes most sense to report the total electrical power consumption (which includes the power for sensing and computing), since it will determine, together with the battery capacity, the all important runtime. In any case, the battery power consumed will always provide an upper bound on joint power, or mechanical power as the battery is the only source of energy in the system.

TABLE III
Experimental statistics

	carpet	linoleum	grass	gravel	rough	single obst.	comp. const.	obst. course
total # of runs	10	11	16	25	32	14	14	26
successful runs	10	10	10	10	16	10	10	10
electronics & hardware problems	-	-	1	5	6	-	-	2
deviation from course	-	1	-	5	7	-	-	5
operator mistake [a]	-	-	5	5	-	3	2	2
stuck on obstacle	-	-	-	-	3	1	2	7

[a] These failure modes include steering in unwanted directions, failure to trigger the timing switch and the power cord wrapping around the legs.

Throughout the experiments, the control parameters were set to fixed values, and these were only modified by the operator via the joystick commands in an attempt to steer the robot along a straight line. The speed command input was used solely for starting and stopping the robot.

Experimental findings are summarized in Table III and Figures 9-8, and discussed in Sections V-C.1 through V-C.6. A detailed account of the setup, measurement protocols and failure modes is presented in the Appendix.

C.1 Forward Locomotion

This first set of experiments documents RHex's maximum velocity, power and specific resistance with the two-stroke open loop controller of Section III while traversing carpet (see Extension 7 for an example run), Linoleum, grass and coarse gravel. The robot moved well over these indoor and outdoor surfaces, with only minor velocity variations between 0.45 m/s and 0.55 m/s as shown in Figure 8. The velocity on Linoleum was lowest due to intermit-

tent slipping, which also causes a larger standard deviation of the runs compared to carpet. In the current prototype, the relatively high natural frequency of the system and the open loop nature of the leg trajectories limit the maximum speed due to out of phase vertical body oscillations, which reduce traction. The surface irregularities of the outdoor grass and gravel surfaces provided improved traction, and therefore average velocities slightly above 0.5 m/s, but also resulted in larger variations between the runs. The specific resistance (power consumption) was lowest on carpet with 2.21 (80 W) and highest on gravel with 3.74 (140 W). We experimented with control parameter settings to reach the maximum robot velocity on office carpet and linoleum, and selected $\mathbf{u} = [0.45, 0.2, 51, 0]$. The grass and gravel surfaces were not tested with these settings prior to the reported experiments. Figure 8 shows the average velocity, power consumption and the specific resistance over ten runs, with standard deviations for all the experiments. All the experimental data as well as the associated analysis scripts can also be found in Extension 8. Table III summarizes the failure modes and statistics for all the experiments described in this Section.

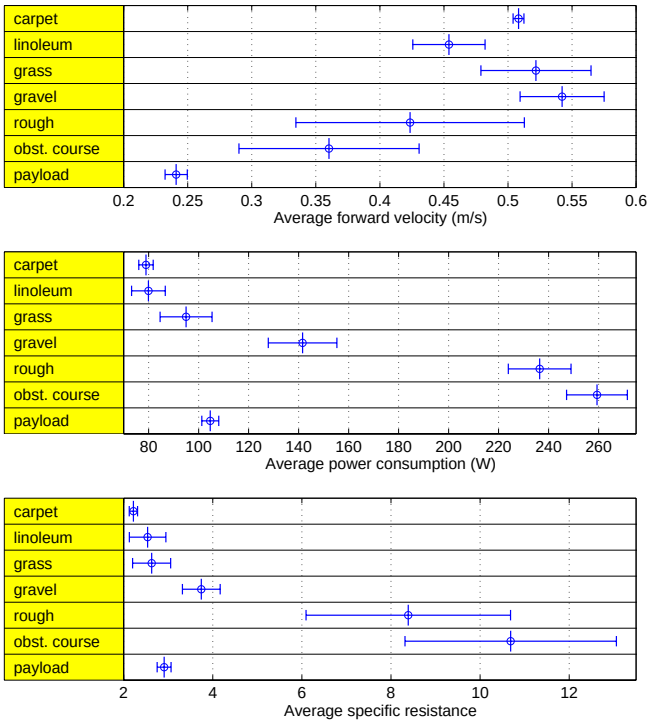

Fig. 8. *Comparison of average forward velocity and energetics for different experiments (also see Extension 8).*

C.2 Turning

As our simulation study had predicted, steering is possible, even though the leg actuation is limited to motion in the sagittal plane only, via differential motion between left and right legs. We selected control parameters which resulted in turns in place and robot speeds up to about 0.4 m/s (see Table IV) on most flat surfaces including carpet, linoleum, grass and gravel. The maximum forward velocity is reduced during turning, because the differential leg motion precipitates the onset of the speed limiting vertical body oscillations. The maximum yaw angular velocities increase almost linearly with forward velocity up to 0.19 rad/s at 0.39 m/s, as illustrated in Figure 9. Interestingly, the resulting turn radius is almost constant with approximately 2 m. Turning in place provides the highest yaw angular velocity of 0.7 rad/s, although it is not possible to directly compare its performance to differential turning, which is a qualitatively different controller. At present, we do not understand completely the relationship between the controller parameters and effective yaw rates, a subject of ongoing research.

TABLE IV
CONTROLLER PARAMETERS FOR TURNING AT DIFFERENT SPEEDS

$\dot{x}$ (m/s)	t_c (s)	t_s (s)	ϕ_s (rad)	ϕ_o (rad)	$\Delta\phi_o$ (rad)	Δt_s (s)
0	1.0	0.6	35	0.0	0.0	0.0
0.16	1.2	0.7	25	0.0	6.0	−0.02
0.28	0.8	0.45	35	0.0	7.5	0.0
0.39	0.53	0.33	40	0.0	6.5	0.0

C.3 Obstacle Crossing

The obstacle crossing capabilities of the simple open loop walking controller were evaluated with two different obstacles - a 15 cm high Styrofoam block and a composite obstacle with a maximum height of 22 cm, as shown in Figures 10 and 11, respectively (also see Extensions 10 and 11). The robot was able to surmount both obstacles, neither sensing them, nor with any modification to the control parameters of the walking experiments. The data in the top portions of the two graphs shows the forward velocity averages before, during and after the obstacle, averaged over ten runs. Surprisingly, the average velocity decreases only slightly as the robot climbs over the obstacle, and increases again afterwards. Since the robot's trajectory over the obstacle de-

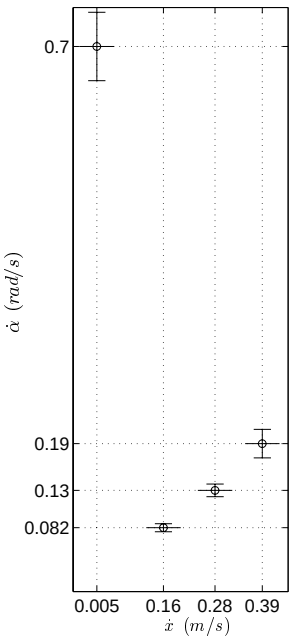

Fig. 9. *Turning yaw rate as a function of forward velocity. See Extension 9 for all the data and analysis scripts associated with the turning experiments.*

pends greatly on how the legs engage it, the standard deviation of the average velocities increases over the obstacle. The average speeds varied most (largest standard deviation) after the composite obstacle, since it depended much on how the robot landed. As a further illustration of the robot's motion, the forward velocity from a particular run, and the robot's body in the sagittal plane at 0.5 s intervals during the same run are shown as well.

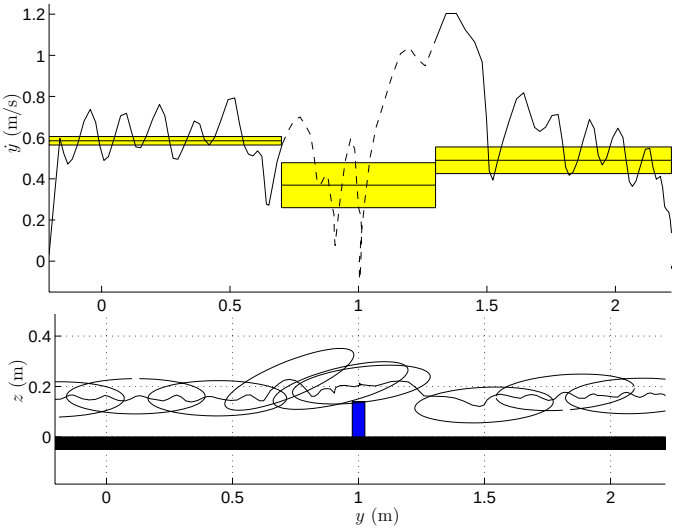

Fig. 10. *Sagittal plane data during simple obstacle crossing. The data in the top portion of the graph shows forward velocity averages and standard deviations before, during and after the obstacle, averaged over ten runs. The solid line is one particular run. The bottom half shows a projection of the robot's body onto the sagittal plane in 0.5 s intervals (horizontal and vertical axes at the same scale). See Extension 12 for all the experimental data and the analysis scripts.*

C.4 Obstacle Course

To demonstrate RHex's rough terrain capabilities, we constructed the obstacle course depicted in Figure 12. It consisted of ten randomly spaced obstacles of 12.2 cm height (that is, 60% of the leg length and exceeding ground clearance by 1.8 cm). This was by far the most challenging of the experiments, requiring the largest number of runs before ten successful completions. Most failures can be attributed to the open loop nature of the walking controller, which had to climb blindly over ten randomly spaced obstacles, sometimes as little as half a body width apart, but all higher than the ground clearance. This had to be done successfully over a distance of 8.13 m, avoiding all the failure modes detailed in the Appendix. Yet, for the ten successful runs, RHex was able to maintain an average velocity of 0.36 m/s over the length of the obstacle course (Figure 8). The best run finished in only 17.78 s, or an average velocity of 0.46 m/s, with a specific resistance of 8.17. The punishing nature of this course is reflected in the power

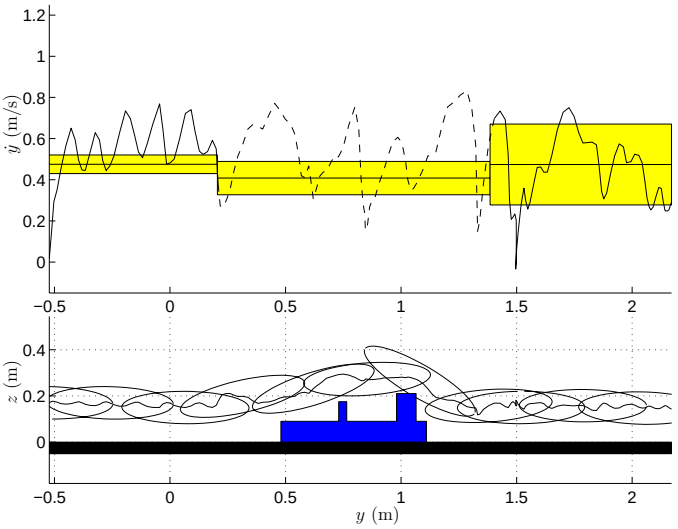

Fig. 11. *Sagittal plane data during composite obstacle crossing. The data in the top portion of the graph shows forward velocity averages and standard deviations before, during and after the obstacle, averaged over ten runs. The solid line is one particular run. The bottom half shows a projection of the robot's body onto the sagittal plane in 0.5 s intervals (horizontal and vertical axes at the same scale). See Extension 13 for all the experimental data and the analysis scripts.*

consumption of more than three times that of walking on carpet, over five times the specific resistance, and a high rate of component breakdown: During the obstacle course experiments, RHex broke three legs, burned several circuit traces, and fractured its frame.

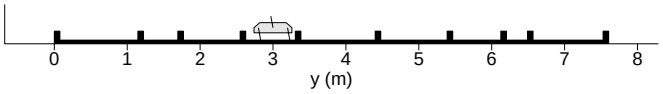

Fig. 12. *Scale drawing of RHex and the obstacle course.*

C.5 Rough Surface

This last rough terrain experiment is an attempt to evaluate RHex's performance in a similar environment to that negotiated by the Blaberus cockroach in [15]. Our efforts at re-creating such a surface at RHex's scale can be evaluated visually in Figure 2 as well as Extensions 3 and 4. To our surprise, RHex was able to traverse this surface with random height variations of up to 20.32 cm (116% leg length, Figure 13) with relative ease at an average velocity of 0.42 m/s (Figure 8). RHex's planar trajectories during the two fastest and the two slowest successful runs are shown in Figure 14. In addition, body state associated with an example run can be found in the multimedia appendix Item 11.

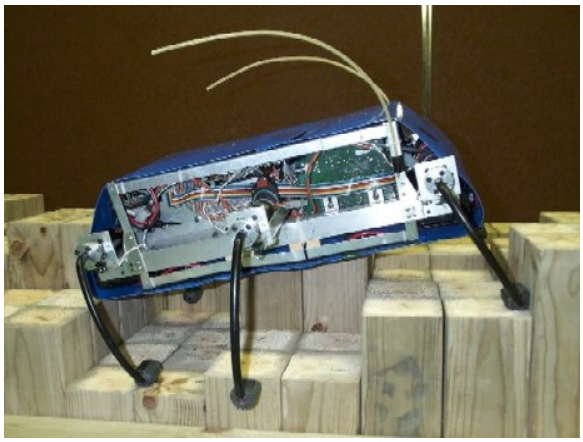

Fig. 13. *Sample profiles of row 6 (columns 8,9 and 10) with RHex statically posed for comparison.*

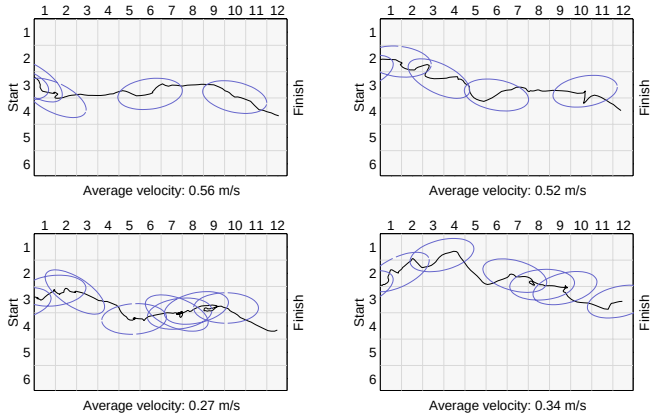

Fig. 14. *The two fastest (top) and the two slowest (bottom) robot trajectories in the horizontal plane as RHex moves over the rough surface. The plots also show projections of the body onto the horizontal plane in 1 s intervals. See Extension 14 for all the experimental data and the asociated analysis scripts.*

C.6 Payload and runtime

To demonstrate RHex's payload capacity, we mounted an additional mass of 7.94 kg (one 10 lb and one 7.5 lb weight-lifting barbell) to the bottom of RHex's body and adjusted the control parameters for lower speed and a small sweep angle ($c_6 = 0.7, 0.2, 14, 0$). The robot was able to transport this additional mass, more than its own total mass, at about half its maximum speed (0.25 m/s) with a specific resistance of about 3. These averages were obtained from ten runs. This payload is close to the limit of the current design, and may not be practical, since the motors are not powerful enough to raise the robot when lying on the floor even when all six legs are used. A careful analysis of tradeoffs between payload and speed in legged systems operating in a quasi-static regime is provided in [23], but is not directly applicable to RHex.

Finally, the endurance of RHex was tested in standby mode, with the motors enabled, and maintaining a standing position, and while walking at maximum speed on carpet. The average standby runtime was 48 minutes, and 18 minutes for continuous walking (both values averaged over 5 successive experiments).

VI. Conclusion

Nimble, robust locomotion over general terrain remains the sole province of animals, notwithstanding our functional prototype, RHex, nor the generally increased recent interest in legged robots. RHex, endowed with only a rudimentary controller, uses what might be termed the engineering equivalent of "preflexes" [8, 15] to negotiate relatively badly broken terrain at relatively high speeds — performance beyond that heretofore reported for autonomous legged vehicles in the archival literature. We are convinced that further systematic application of certain operational principles exhibited by animals will achieve significant increases in RHex performance, and inform the evolution of the underlying mechanical design of future prototypes as well. To conclude the paper, we provide a brief sketch of these principles and how they may be applied.

Accumulating evidence in the biomechanics literature suggests that agile locomotion is organized in nature by recourse to a controlled bouncing gait wherein the "payload", the mass center, behaves mechanically as though it were riding on a pogo stick [7]. While Raibert's running machines were literally embodied pogo sticks [30], more utilitarian robotic devices such as RHex must actively anchor such templates within their alien morphology if the animals' capabilities are ever to be successfully engineered [16]. We have previously shown how to anchor a pogo stick template in the more related morphology of a four degree of freedom monopod [32]. The extension of this technique to the far more distant hexapod morphology surely begins with the adoption of an alternating tripod gait, but its exact details remain an open question, and the "minimalist" RHex design (only six actuators for a six degree of freedom payload!) will likely entail additional compromises in its implementation. Moreover, the only well understood pogo stick is the Spring Loaded Inverted Pendulum [34], a two degree of freedom sagittal plane template that ignores body attitude and all lateral degrees of freedom. Recent evidence of a horizontal pogo stick in sprawled posture animal running [25] and subsequent analysis of a proposed lateral leg spring template to represent it [33] advance the prospects for developing a spatial pogo stick template in the near future. Much more effort remains before a functionally biomimetic six degree of freedom "payload" controller is available, but we believe that the present understanding of the sagittal plane can already be used to significantly increase RHex's forward speed, and, as well, to endow our present prototype with an aerial phase.

Appendix

I. Index to multi-media Extensions

TABLE V
Index to multi-media extensions

Ext.	Media type	Description
1	Video	RHex traversing simple outdoor obstacles
2	Video	Demonstration of RHex's leg compliance
3	Video	Example simulation with SimSect
4	Video	Basic walking gait
5	Video	RHex traversing a single high styrofoam obstacle
6	Data	Data and analysis scripts for the single obstacle experiments
7	Video	RHex traversing a composite obstacle
8	Data	Data and analysis scripts for the composite obstacle experiments
9	Video	Front view of RHex over the rough surface obstacle
10	Video	Top view of RHex over the rough surface obstacle
11	Data	Data and analysis scripts for the rough surface experiments
12	Video	RHex traversing a challenging indoor obstacle
13	Data	Data and analysis scripts for turning experiments
14	Data	Power, speed and specific resistance data and analysis scripts for all the experiments.

The multi-media extensions to this article (see Table V) can be found online by following the hyperlinks from `www.ijrr.org`.

II. Details of the Experimental Setup and Failure Modes

A. Forward Locomotion

We ran the robot over carpet, linoleum, grass and gravel. The carpet and linoleum surfaces were standard office floors found close to the lab. The grass was wet on the day of the experiment and showed height variations of about 2 cm. The gravel patch contained fairly large gravel pieces (see Figure 1) between three and eight cm diameter. For all the experiments, the robot was driven over a test stretch of 2 m. In order to obtain precise timing and to synchronize the data logging with the test stretch, a switch was mounted in the front of the robot, which was triggered as the robot ran into a Styrofoam panel held at the beginning and the end of the test stretch. The runs over each surface were repeated until ten successful runs were obtained. The average velocity and power consumption for each run was then computed with the available data.

Ten successive experiments were run for the carpet surfaces with no failures. One run on the Linoleum floor was discarded, since the robot deviated too much from the straight line. A total of 16 runs on grass were necessary, with six runs discarded. In five runs, the operator failed to align the start or stop trigger panel properly, and the front legs pushed it aside, preventing the switch to be actuated. One run was abandoned due to R/C noise in the remote control command input. Gravel was more challenging - of the 25 runs, five were discarded because the robot deviated too much from a straight line, five due to the operator missing the trigger switch, one due to remote control noise, and four because the front switch broke on impact with the trigger panel.

B. Turning

The turning experiments were run on carpet. In order to reduce the data processing for this set of experiments, only six runs were processed in this fashion for each forward velocity, instead of the usual ten. Only few runs were discarded due to noise in the remote control which interfered with the velocity and/or the steering command.

C. Obstacle Crossing

The first obstacle was a 1.22 m long strip of 3" (7.62cm) thick Styrofoam board, a standard insulating construction material, cut to 15 cm height. This represents 80% of the robot's leg length and exceeds it's 10.5 cm ground clearance by 4.6 cm, or almost 50%. The Styrofoam was chosen for this experiment and the random obstacle course described below for its ready availability, low cost, and ease of cutting. It is softer than wood, yet hard enough that the robot does not deform it. The second obstacle was built from construction lumber and consisted of a 10 cm high and 63 cm wide base (as viewn in the sagittal plane) on top of which a 8.5 cm high and 3.5 cm wide block was mounted at a distance of 25 cm from the front and a 12.5 cm high and 8.5 cm wide second block was mounted at a distance of 50 cm from the front. In both experiments the control parameters were the same as in the walking experiments above. All data shown was obtained by the visual tracking procedure described in Section V-B, with the camera oriented for a perpendicular view of the sagittal plane. The average forward velocity of each run was obtained before, over, and after the obstacle.

Fourteen successive experiments were required and logged for both obstacles. From the runs over the first obstacle, the robot failed to surmount it only once, but the vision post processing algorithm failed to extract reliable position data for three successful runs, when the robot's di-

rection after obstacles deviated significantly from straight path. From the fourteen successive runs over the composite obstacle, the robot failed twice to surmount the obstacle, and the vision post processing failed to extract data from the post-obstacle portion of two runs.

D. Obstacle Course

The experimental setup for the obstacle course consisted of ten randomly spaced obstacles of 12.2 cm height. The free spaces between the ten 3" (7.62cm) wide Styrofoam blocks were 1.07, 0.47, 0.78, 0.68, 1.02, 0.91, 0.66, 0.29 and 0.96 m, selected between 0.5 and 2 body lengths from a uniform random distribution. Thus the total obstacle course extended over 8.13 m, which also includes one half body length before and after the course. The time between start and finish was measured via a stopwatch. During these experiments an operator attempted to keep the robot on course using the limited directional control described above. Nevertheless, the directional disturbances due to the obstacles caused the robot at times to veer towards the lateral limits of the 1.2 m wide course. In those instances, operators who followed the robot along the course, placed a Styrofoam panel along the lateral limits to make up for the lack of side walls. When the collision angle with these walls was sufficiently small, the robot re-aligned itself with the course.

Due to the large number of runs required for this experiment, and the high power requirements, we made an exception and ran the robot from higher capacity external batteries via an umbilicus. This greatly reduced the experimental effort by eliminating the need to recharge and exchange the on-board batteries. However, no performance improvement resulted from this arrangement, compared to running off freshly charged on-board batteries. The on-board batteries were kept in place to maintain the total robot mass.

A total of 26 successive experiments on the obstacle course were recorded. Of these, 16 were discarded for the following reasons: The robot turned itself sideways beyond quick recovery (2), shut itself off (1), required operator intervention through the R/C unit, such as turning in place or short reversal of direction to complete the course (3), turned itself on its back either by climbing up against the side walls (1) or the obstacle (3), wrapped the power cord around the legs (1), ends up "sitting" aligned with and on top of an obstacle, unable to reach the ground (3), or burned electrical circuits (1). The remaining eleven runs were used to calculate the velocity, power and specific resistance data shown in Figure 8.

E. Rough Surface

In order to re-create Full's rough surface [15], we compared the height distribution of his environment [14] to checkerboard arrays of randomly uniformly distributed block heights. When scaled to RHex's dimensions, we decided that a height variation of between 4" (10.16 cm) and 12" (30.48 cm), or 1.16 leg lengths was a good match (Figure 15). To simplify cutting by a local lumber yard, the block heights were discretized to 1" (2.54 cm) increments. The block width of 7" (17.78 cm) permitted the use of four standard 3.5"x3.5" (8.89cm x 8.89 cm) cross section lumber per checkerboard block. The total surface consisted of 72 blocks (6 by 12) thus requiring 288 individually cut lumber sections. The robot was run in the direction of the 12 block length of the surface, with wall panels on each side. Its cartesian position and orientation, projected onto the horizontal plane, was measured with the visual tracking setup described in the steering experiment, above.

	1	2	3	4	5	6	7	8	9	10	11	12
1	12"	8"	4"	7"	11"	12"	9"	6"	6"	7"	7"	8"
2	9"	4"	11"	8"	8"	10"	11"	5"	12"	6"	9"	12"
3	9"	8"	10"	9"	6"	10"	8"	5"	4"	7"	5"	6"
4	10"	6"	12"	10"	9"	11"	8"	8"	9"	6"	5"	8"
5	5"	11"	10"	10"	10"	12"	5"	11"	8"	10"	6"	8"
6	4"	9"	7"	8"	10"	8"	5"	6"	9"	12"	9"	11"

Start

Finish

Fig. 15. *Height distribution over the rough surface*

We carried out 32 experiments on this surface, with a success rate of 50%. During the unsuccessful runs, the robot either ran head-on into a side wall or into one of the isolated posts (typically the isolated high block with coordinates 2,9 in Figure 15 (3), broke a leg (twice), hit one of the walls (3), had to back up and continue forward (4). Also, four of the experiments did not complete due of R/C failure. From the 16 experiments that were successfully recorded, we have used 10 with the cleanest vision data to facilitate the post-processing.

Acknowledgements

This work was supported in part by DARPA/ONR Grant N00014-98-1-0747. Bob Full consulted on many of the design decisions and provided numerous tutorial explanations of the biomechanics literature. Greg Sharp built the software for the processing of our vision data. Jim Berry helped in setting up and running many of the experiments. Noah Cowan offered very helpful advice concerning modeling and simulation. Liana Mitrea made invaluable contributions in the mechanical construction of the hexapod platform.

References

[1] M. Ahmadi and M. Buehler, "The ARL Monopod II Running Robot: Control and Energetics," in *IEEE Int. Conf. Robotics and Automation*, Detroit, MI, May 1999, pp. 1689–1694.

[2] R. Altendorfer, U. Saranli, H. Komsuoglu, D. E. Koditschek, Jr. H. B. Brown, M. Buehler, N. Moore, D. McMordie, and R Full, "Evidence for spring loaded inverted pendulum running

in a hexapod robot," in *International Symposium on Experimental Robotics*, Hawaii, 2000.

[3] C. Angle, "Genghis: A six-legged autonomous walking robot 1989, SB thesis.

[4] C. Angle, "Design of an artificial creature," M.S. thesis, Massachusetts Institute of Technology, Cambridge, MA, 1991.

[5] J. E. Bares and D. S. Wettergreen, "Dante II: Technical Description, results and lessons Learned," *International Journal of Robotics Research*, vol. 18, no. 7, pp. 1–29, July 1999.

[6] M. Binnard, "Design of a small pneumatic walking robot," M.S. thesis, Massachusetts Institute of Technology, Cambridge, MA, 1995.

[7] R. Blickhan and R. J. Full, "Similarity in multilegged locomotion: Bouncing like a monopode.," *Journal of Comparative Physiology*, vol. A. 173, pp. 509–517, 1993.

[8] I. E. Brown and G. E. Loeb, "A reductionist approach to creating and using neuromusculoskeletal models," in *Biomechanics and Neural Control of Movement*. Springer-Verlag, In press.

[9] M. Buehler, R. Battagila, A. Cocosco, G. Hawker, J. Sarkis, and K. Yamazaki, "SCOUT: A simple quadraped that walks, climbs and runs," in *Proceedings of the IEEE International Conference On Robotics and Automation*, Leuven, Belgium, May 1998, pp. 1707–1712.

[10] M. Buehler, A. Cocosco, K. Yamazaki, and R. Battaglia, "Stable open loop walking in quadruped robots with stick legs," in *Proceedings of the IEEE International Conference On Robotics and Automation*, Detroit, Michigan, May 1999.

[11] H. J. Chiel, R. D. Beer, R. D. Quinn, and K. S. Espenchied, "Robustness of a distributed neural network controller for locomotion in a hexapod robot," *IEEE Transactions on Robotics and Automation*, vol. 6, no. 3, pp. 293–303, 1992.

[12] J. E. Clark, J. G. Cham, S. A. Bailey, E. M. Froehlich, P. K. Nahata, R. J. Full, and M. R. Cutkosky, "Biomimetic Design and Fabrication of a Hexapedal Running Robot," in *Proceedings of the IEEE International Conference On Robotics and Automation*, Seoul, Korea, May 2001.

[13] Michael J. Coleman, Anindya Chatterjee, and Andy Ruina, "Motions of a rimless spoked wheel: a simple three-dimensional system with impacts.," *Dynamics and Stability of Systems.*, vol. 12, no. 3, pp. 139–159, 1997.

[14] R. J. Full. Personal communication.

[15] R. J. Full, K. Autumn, J. I. Chung, and A. Ahn, "Rapid negotiation of rough terrain by the death-head cockroach," *American Zoologist*, vol. 38, pp. 81A, 1998.

[16] R. J. Full and D. E. Koditschek, "Templates and Anchors: Neuromechanical Hypotheses of Legged Locomotion on Land," *Journal of Experimental Biology*, vol. 202, pp. 3325–3332, 1999.

[17] G. Gabrielli and T. H. von Karman, "What price speed?," *Mechanical Engineering*, vol. 72, no. 10, pp. 775–781, 1950.

[18] H. Goldstein, *Classical Mechnanics*, Addison-Wesley, 1980.

[19] P. Gregorio, M. Ahmadi, and M. Buehler, "Design, control and energetics of an electrically actuated legged robot," *IEEE Trans. Systems, Man, and Cybernetics*, vol. 27, no. 4, pp. 626–634, Aug 1997.

[20] H. G. Grimm Animated Toy, US Patent 2,827,735; 1958.

[21] S. Hirose, "A study of design and control of a quadruped walking machine.," *International Journal of Robotics Research*, vol. 3, no. 2, pp. 113–133, 1984.

[22] E. R. Honeywell Walking Tractor, US Patent 1,375,752; 1920.

[23] M. Z. Huang and K. J. Waldron, "Relationship between payload and speed in legged locomotion systems," *IEEE Transactions on Robotics and Automation*, vol. 6, no. 5, pp. 570–577, October 1990.

[24] Interelectric AG, Sachseln, Switzerland, *Maxon Motor Catalog*, 1997/98, www.maxon.com.

[25] T. M. Kubow and R. J. Full, "The role of the mechanical system in control: A hypothesis of self-stabilization in hexapedal runners," *Phil. Trans. R. Soc. Lond.*, vol. B. 354, pp. 849–862, 1999.

[26] Mattel's *Major Matt Mason's* #6304 Space Crawler http://www.wildtoys.com/MMMPage/MattelPlaysets/mmm3part1.html.

[27] NSF Institute for Mathematics and Its Applications Spring 1998 Workshop on Animal Locomotion and Robotics. June 1-5 1998, http://www.ima.umn.edu/dynsys/spring/dynsys10.html.

[28] D. Papadopoulos and M. Buehler, "Stable running in a quadruped robot with compliant legs," in *Proceedings of the IEEE International Conference On Robotics and Automation*, San Francisco, CA, April 2000.

[29] D. R. Pugh, E. A. Ribble, V. J. Vohnout, T. E. Bihari, T. M. Walliser, M. R. Patterson, and K. J. Waldron, "Technical description of the adaptive suspension vehicle," *International Journal of Robotics Research*, vol. 9, no. 2, pp. 24–42, April 1990.

[30] M. H. Raibert, *Legged robots that balance*, MIT Press, Cambridge MA, 1986.

[31] U. Saranli, *SimSect Programmer's Manual*, The University of Michigan, 1999, In preparation.

[32] U. Saranli, W. J. Schwind, and D. E. Koditschek, "Toward the Control of a Multi-Jointed, Monoped Runner," in *Proceedings of the IEEE International Conference On Robotics and Automation*, Leuven, Belgium, May 1998, vol. 3, pp. 2676–82.

[33] J. Schmitt and P. Holmes, "Mechanical models for insect locomotion I: Dynamics and stability in the horizontal plane.," *Biological Cybernetics*, vol. submitted, 1999.

[34] W. J. Schwind and D. E. Koditschek, "Approximating the stance map of a 2-dof monoped runner," *Journal of Nonlinear Science*, vol. 10, pp. 533–568, 2000.

[35] K. J. Waldron and V. J. Vohnout, "Configuration design of the Adaptive Suspension Vehicle.," *International Journal of Robotics Research*, vol. 3, no. 2, pp. 37–48, 1984.